NANO LETTERS

2007
Vol. 7, No. 6
1655−1663

Biaxially Stretchable "Wavy" Silicon Nanomembranes

Won Mook Choi,[†] Jizhou Song,[‡] Dahl-Young Khang,[†] Hanqing Jiang,[§] Yonggang Y. Huang,[‡] and John A. Rogers*,[†]

Department of Materials Science and Engineering, Department of Chemistry, Beckman Institute for Advanced Science and Technology, and Frederick Seitz Materials Research Laboratory, University of Illinois at Urbana-Champaign, Urbana, Illinois 61801, Department of Mechanical Science and Engineering, University of Illinois at Urbana-Champaign, Urbana, Illinois 61801, and Department of Mechanical and Aerospace Engineering, Arizona State University, Tempe, Arizona 85287

Received March 15, 2007; Revised Manuscript Received April 18, 2007

ABSTRACT

This Letter introduces a biaxially stretchable form of single crystalline silicon that consists of two dimensionally buckled, or "wavy", silicon nanomembranes on elastomeric supports. Fabrication procedures for these structures are described, and various aspects of their geometries and responses to uniaxial and biaxial strains along various directions are presented. Analytical models of the mechanics of these systems provide a framework for quantitatively understanding their behavior. These classes of materials might be interesting as a route to high-performance electronics with full, two-dimensional stretchability.

Electronics that offer mechanically bendability are of interest for applications in information display, X-ray imaging, photovoltaic devices, and other systems.[1] Reversible stretchability is a different and much more technically challenging mechanical characteristic that would enable device possibilities that cannot be realized with electronics that are only bendable, such as smart surgical gloves,[2] electronic eye cameras,[3] and personal health monitors.[4] In one approach to electronics of this type, stretchable wires interconnect rigid device islands to provide circuit level stretchability with device components that are not stretchable.[5] In an alternative strategy, certain structural forms of thin single-crystal semiconductor and other electronic materials allow stretchability in the devices themselves. Recent demonstrations[6,7] involved the use of buckled, one-dimensional "wavy" geometries in nanoribbons (thicknesses between tens and hundreds of nanometers and widths in the micrometer range) of silicon and gallium arsenide to achieve uniaxial stretchability in metal oxide semiconductor field effect transistors (MOSFETs), metal semiconductor field effect transistors (MESFETs), pn junction diodes, and Schottky diodes. This paper shows that nanomembranes of similar materials can be formed into two-dimensional (2D) wavy geometries to provide full 2D stretchability. The fabrication procedures for such systems are described, together with detailed experimental characterization and analytical modeling of their mechanical response.

Figure 1 schematically illustrates the steps for forming two dimensionally stretchable Si nanomembranes on elastomeric supports. For the work described here, these membranes were fabricated from silicon-on-insulator (SOI) wafers (Soitec, Inc., p-type) starting with the formation of a square array of holes in the top silicon (∼2.5 μm diameter, and ∼25 μm pitch), by defining suitable patterns of photoresist by photolithography and then removing the exposed silicon by reactive ion etching (PlasmaTherm RIE, SF_6 40 sccm, 50 mTorr, 100 W). This same step defined the overall lateral dimensions of the membranes which, for the samples reported here, were in the range of 3−5 mm square. The thicknesses were between 55 and 320 nm. Immersing the etched samples in concentrated hydrofluoric acid (HF 49%) removed the buried SiO_2 layer (145∼1000 nm thick); washing in acetone removed the photoresist. Casting and curing prepolymers of poly(dimethylsiloxane) (PDMS) against polished silicon wafers generated flat, elastomeric substrates (∼4 mm thick). Exposure to an ozone environment created

* To whom correspondence should be addressed. E-mail: jrogers@uiuc.edu. Tel: 1-217-244-4979. Fax: 1-217-333-2736.

[†] Department of Materials Science and Engineering, Department of Chemistry, Beckman Institute for Advanced Science and Technology, and Frederick Seitz Materials Research Laboratory, University of Illinois at Urbana-Champaign.

[‡] Department of Mechanical Science and Engineering, University of Illinois at Urbana-Champaign.

[§] Department of Mechanical and Aerospace Engineering, Arizona State University.

10.1021/nl0706244 CCC: $37.00
Published on Web 05/08/2007

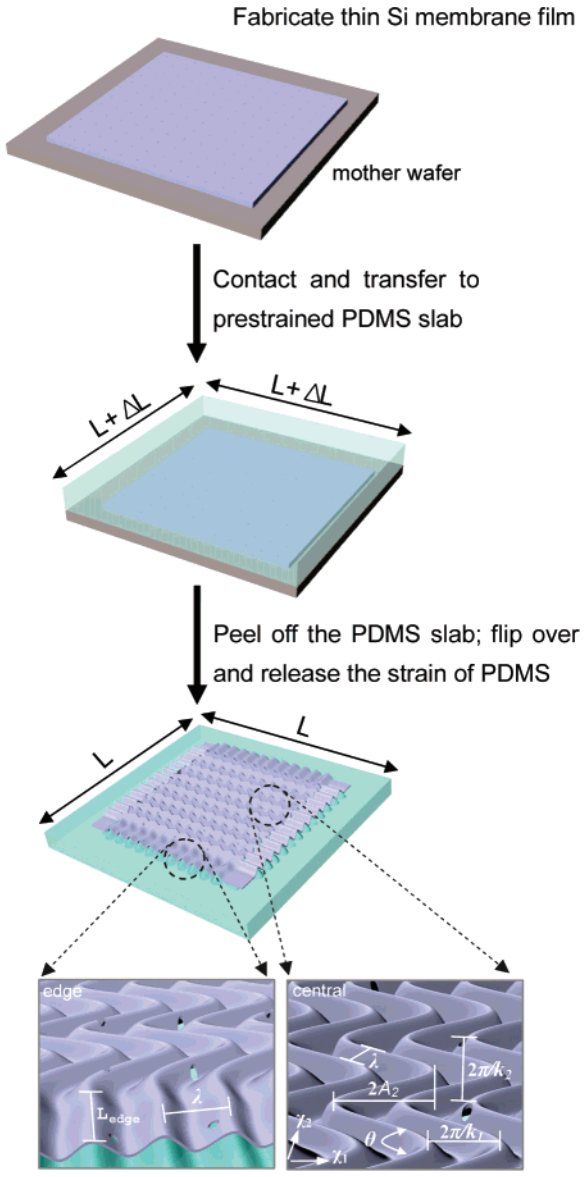

Figure 1. Schematic illustration of steps for fabricating two-dimensional, "wavy" semiconductor nanomembranes on elastomeric supports.

by intense ultraviolet light (240−260 nm) for 5 min converted the hydrophobic PDMS surface (−CH_3 and −H end groups) to a hydrophilic state (−OH and −O−Si−O− end groups).[8] Heating such an activated PDMS substrate briefly at 70−180 °C in a convection oven induced a controlled degree of isotropic thermal expansion. Contacting this element to the processed SOI wafer and then peeling it off again transferred the entire nanomembrane to the PDMS. Continued heating in the convection oven for a few minutes facilitated the formation of strong adhesive bonds between the membrane and the PDMS.[7] In the final step, the nanomembrane/PDMS structure was cooled to room temperature (ca. 25 °C) to release the thermally induced prestrain ($\Delta L/L$). This process led to the spontaneous formation of two-dimensional (2D) wavy structures of relief in the Si nanomembrane and the near surface region of the PDMS. These structures exhibited different behaviors near the edges, where one-dimensional periodic waves predominate, at the inner regions, where two-dimensional herringbone layouts are typically observed, and near the centers, where disordered herringbone structures often occur. The herringbone region is characterized by the distance between adjacent peaks in the waves, which we refer to as the short wavelength λ, the amplitude of wave A_1 (not shown in Figure 1), and a longer distance $2\pi/k_2$ (along the x_2 direction), associated with the separation between adjacent "jogs" in the herringbone structure, which we refer to as the long wavelength. Other characteristic length are the 'jogs' wavelength $2\pi/k_1$ (along the x_1 direction, normal to the long wavelength direction x_2), the amplitude A_2 of the jogs, the jog angle θ. The bottom frames of Figure 1 illustrate these features schematically.

Parts a−f of Figure 2 show optical micrographs collected at different stages during the formation of herringbone waves, for the case of a nanomembrane with 100 nm thickness (lateral dimension of ca. 4 × 4 mm^2) and thermal prestrain (defined by heating to 150 °C) of ∼3.8%.[9] These images indicate structure formation in two stages, the first of which involves predominantly one-dimensional waves over large areas followed by bending of these wave structures to form, ultimately, compact herringbone layouts at full cooling (Figure 2d−f). Figure 2h shows the time evolution of both characteristic wavelengths. The short wavelength tends to decrease as the cooling leads to progressively larger compressive strain on the silicon due to the relatively larger thermal contraction of the PDMS. In particular, this value decreases from 17−18 μm in the initial stages to ∼14.7 μm when the herringbone structure becomes prominent and finally to ∼12.7 μm in the fully cooled state. This wavelength is uniform (∼5% variation) over large areas. By contrast, the long wavelength associated with the herringbone layout exhibits a broad range of values, as is evident from the image in Figure 2g. Measurements at ∼100 spots across this sample yield a distribution of values, summarized in the histogram of Figure 2g. The herringbone structure can be represented by an out-of-plane displacement $w = A_1 \cos[k_1x_1 + k_1A_2 \cos(k_2x_2)]$ (Figure S2). Here the coefficients, amplitude of wave A_1, long wavelength $2\pi/k_2$, jogs wavelength $2\pi/k_1$ and the amplitude A_2 of the jogs are determined by analysis for a particular membrane thickness, mechanical properties of the film, and substrate. The short wavelength λ is $(2\pi/k_1)\sin(\theta/2)$. The modeling uses the Si strain, as determined from measured contour lengths and periods of the wavy structures, as the applied prestrain, instead of the thermal prestain (Figure S3). The actual strain that deforms the Si is typically somewhat smaller than the estimated thermal prestain, due possibly to a loading effect of the Si on the PDMS. The Si strain, for example, is 2.4% at the thermal prestrain of 3.8%. For such a displacement w, the stress, strain, and displacement fields in the Si film can be obtained in terms of A_1, k_1, A_2, and k_2 from the Von Karman plate theory.[10] The fields in the PDMS substrate are obtained from 3D elasticity theory.[11] Minimizing the total energy, which consists of the membrane energy and bending energy in the Si film and the elastic energy in the PDMS substrate,[12,13] gives A_1, k_1, A_2, and k_2. The Young's modulus and Poisson's ratio of Si[9b]

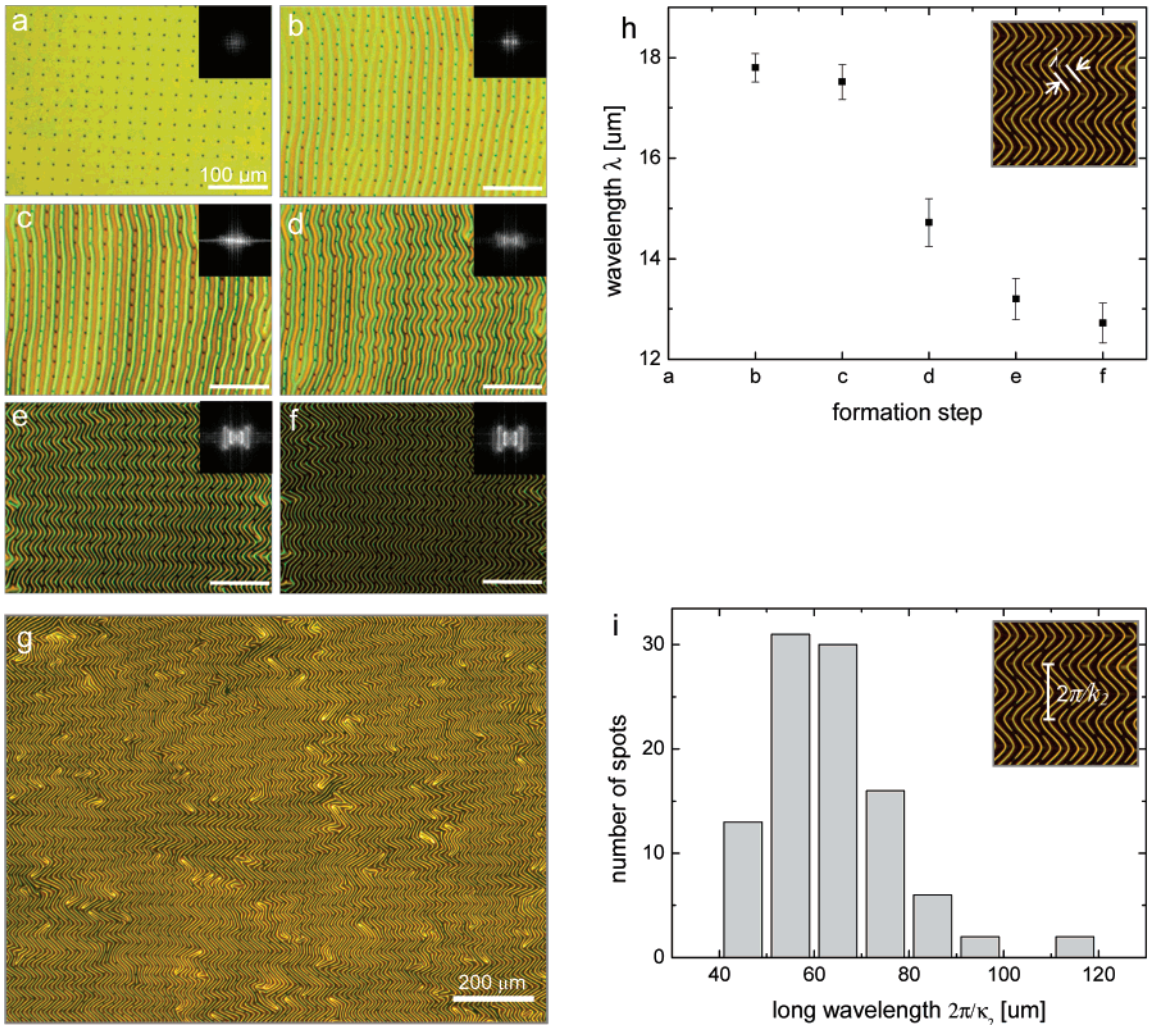

Figure 2. (a−f) Optical micrographs of 2D wavy structures in silicon nanomembranes at various stages during their formation. The insets show two-dimensional power spectra. (g) Image of the fully developed structure, at low magnification. For this sample, the thickness of the silicon is 100 nm with the lateral dimension of ca. 4×4 mm^2, the substrate is PDMS, and the thermally induced prestrain is 3.8%. (h) Plot of the short wavelength corresponding to frames (a−f) and (i) histogram of long wavelength evaluated at various points from frame (g).

and PDMS[14] are $E_{Si} = 130$ GPa, $\nu_{Si} = 0.27$, $E_{PDMS} = 1.8$ MPa, and $\nu_{PDMS} = 0.5$. Both the experiments and model give the jog angle θ to be about 90°. The short wavelength given by the theory is 12.4 μm at 2.4% biaxial prestain, which agrees well with the experimental results above. The large variation in the long wavelength $2\pi/k_2$ is also predicted by the theoretical calculation, from 30 to 60 μm.

Figure 3 presents atomic force microscope (AFM) and scanning electron microscope (SEM) images of structures similar to those illustrated in the fully cooled state of Figure 2. These images clearly show that the herringbone patterns are characterized by zigzag structures that define two characteristic directions, even though the compressive strain is completely isotropic. The herringbone structures represent a minimum elastic energy configuration that reduces the overall in-plane stress in the system and relieves biaxial compression in both directions. This geometry is, therefore, preferred over large areas, compared to the "checkerboard" and 1D wave layouts[12] because the herringbone mode is the only one of these three modes that relaxes the in-plane stress in all directions without incurring significant stretch energy. Only in the immediate vicinity of the jogs is significant stretch induced. The 1D mode lowers the prestress only in one direction. The checkerboard mode lowers the stress in all directions, but it produces significant stretch energy accompanying the bending.

The two linecuts extracted from the AFM images indicate periodic, although only approximately sinusoidal, relief profiles along the jogs direction (profile i) and perpendicular to waves (profile ii). The λ and A_1 of waves, determined from profile ii, are 12.8 and 0.66 μm, respectively. The λ given by theoretical analysis, 12.4 μm, is similar with the experimental data; however, the A_1 from theoretical analysis is 0.90 μm, somewhat higher value than the experimental results. The SEM images show clearly the intimate bonding between the membrane and the PDMS, as evidenced by the behavior of the sample near the small holes in the silicon in both the raised and recessed regions of the waves. These images also indicate that the wave structures are completely uncorrelated to the position of these holes, since the hole size of 2.5 μm is much smaller than the characteristic wavelengths of the deformation modes in our experiments. Studies of the dependence of the geometry of the wavy structures on the thickness of the silicon can provide

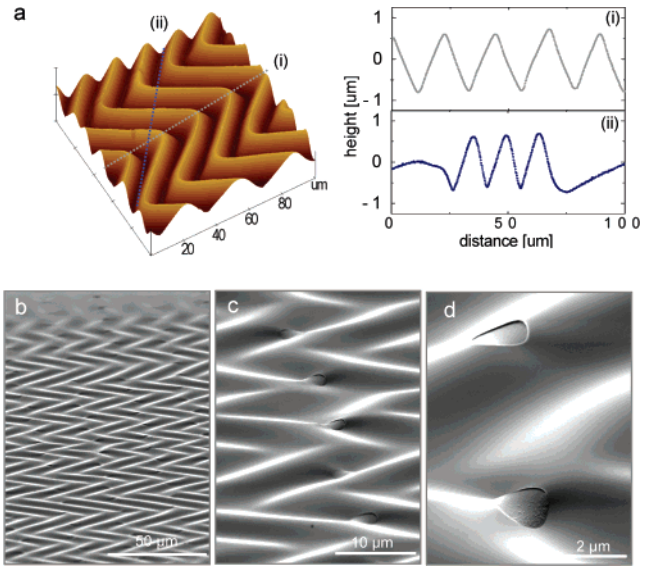

Figure 3. (a) AFM and (b−d) SEM images (tilt angle = 60°) of a 2D wavy Si nanomembrane on PDMS. The thickness of the silicon is 100 nm, and the thermal prestrain is 3.8%. These images highlight the highly periodic nature of the wavy patterns, the good bonding between the Si and the PDMS as evidenced by the intimate contact visible at the edges of the Si and PDMS near the holes etched in the Si, and the lack of correlation between the positions of the wave structures and these holes.

additional insights into the physics and further validate the mechanics models. Figure 4 shows some results, including optical micrographs and wavelengths and amplitudes of wave structures formed in membranes with different thicknesses for similar thermal strains. For 100 nm thickness, the λ and A_1 of waves are 12.6 (±0.37) and 0.64 (±0.07) μm, respectively, and for 320 nm thick, they are 45.1 (±1.06) and 1.95 (±0.18) μm. These values correspond reasonably well with theoretical calculations, which yield the λ and A_1 are 12.4 and 0.90 μm for the 100 nm case and 45.1 and 3.29 μm, respectively, for the 320 nm case.

These wavy membranes provide true stretchability for strains in various in-plane directions, as opposed to the one-dimensional stretchability provided by previously described ribbon geometries.[6,7] To investigate this aspect, we performed uniaxial tensile stretching tests along different directions using a calibrated mechanical stage and a 2D stretchable membrane prepared with a thermally induced prestrain of 3.8%. Figure 5 provides some images. In case i, tensile stain (ϵ_{st}) applied along the direction of the long waves caused the herringbone structure to "unfold" (ϵ_{st} = 1.8%), gradually leading to a 1D wavy geometry at a fully stretched state (ϵ_{st} = 3.8%). This stretching induces, by the Poisson effect, a compressive strain in the orthogonal direction with an amplitude roughly equal to half of the tensile strain. This compressive strain can be accommodated by compression of the wavy structures in this direction. Upon release of the applied tensile strain, the original herringbone waves recovered to exhibit structures quite similar to the original.[15] (Figure S4 shows optical micrographs collected after 5, 10, and 15 stretching cycles.)

Tensile strains applied in a diagonal direction (case ii), showed similar structural changes although at full stretching

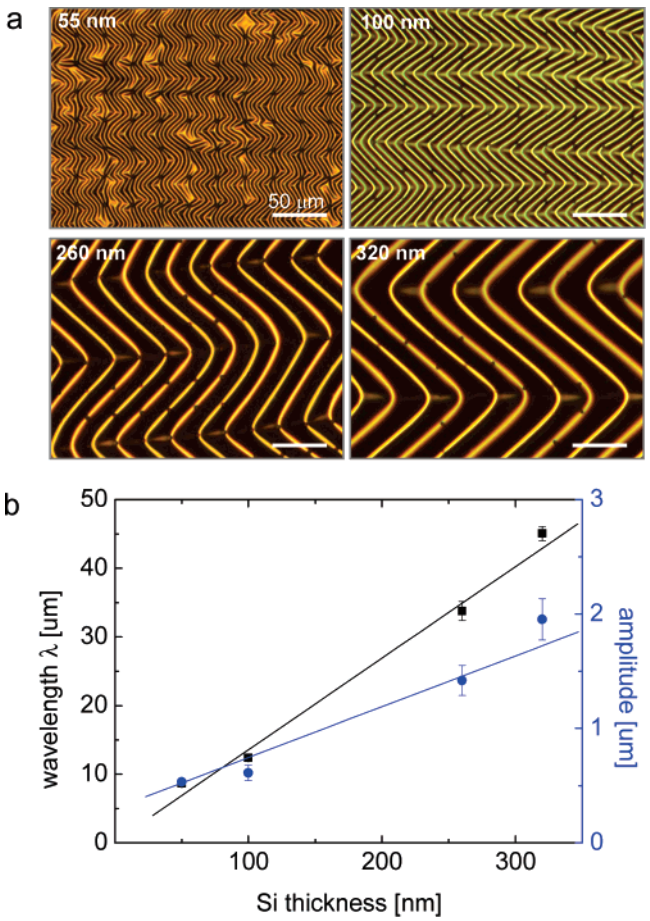

Figure 4. (a) Optical micrographs of 2D wavy Si nanomembranes with various thickness (55, 100, 260, 320 nm) on PDMS, formed with a thermal prestrain of 3.8%, and (b) dependence of the short wavelength and amplitude on Si thickness.

the 1D wave structures aligned along a direction defined by the applied strain, rather than the initial geometry. For the perpendicular case iii, at small strain (ϵ_{st} = 1.8%) certain portions of the sample lose completely the herringbone layout to yield new 1D waves along the stretching direction. With increasing strain, more regions undergo this transformation until the entire area consist of these oriented 1D waves. These newly formed 1D waves are perpendicular to the orientation of the original waves; upon release, they simply bend to create a disordered herringbone-like geometry. For all cases shown in Figure 5b, the wavelength increases with tensile strain and recovers to its initial value upon the release, even though compressive stresses are induced in the orthogonal direction by the Poisson effect. This behavior arises from an increase of λ induced by the unfolding of the herringbone waves that is larger than the decrease in this wavelength caused by the Poisson effect. (Figure S5) For case i, the jogs wavelength, $2\pi/k_1$ (Figure S5a) decreases to $2\pi/k'_1$ (Figure S5b), i.e., $k'_1 > k_1$, under the applied tensile strain, ϵ_{st}, due to the Poisson effect. However, the corresponding jog angle θ' is larger than the angle θ due to the unfolding of the herringbone structure. The short wavelength $\lambda = (2\pi/k_1)\sin(\theta/2)$ becomes $\lambda' = (2\pi/k'_1)\sin(\theta'/2)$, which may be larger than λ when the effect of angle change overcomes the Poisson effect. Our theoretical model gives λ = 12,4, 14.6,

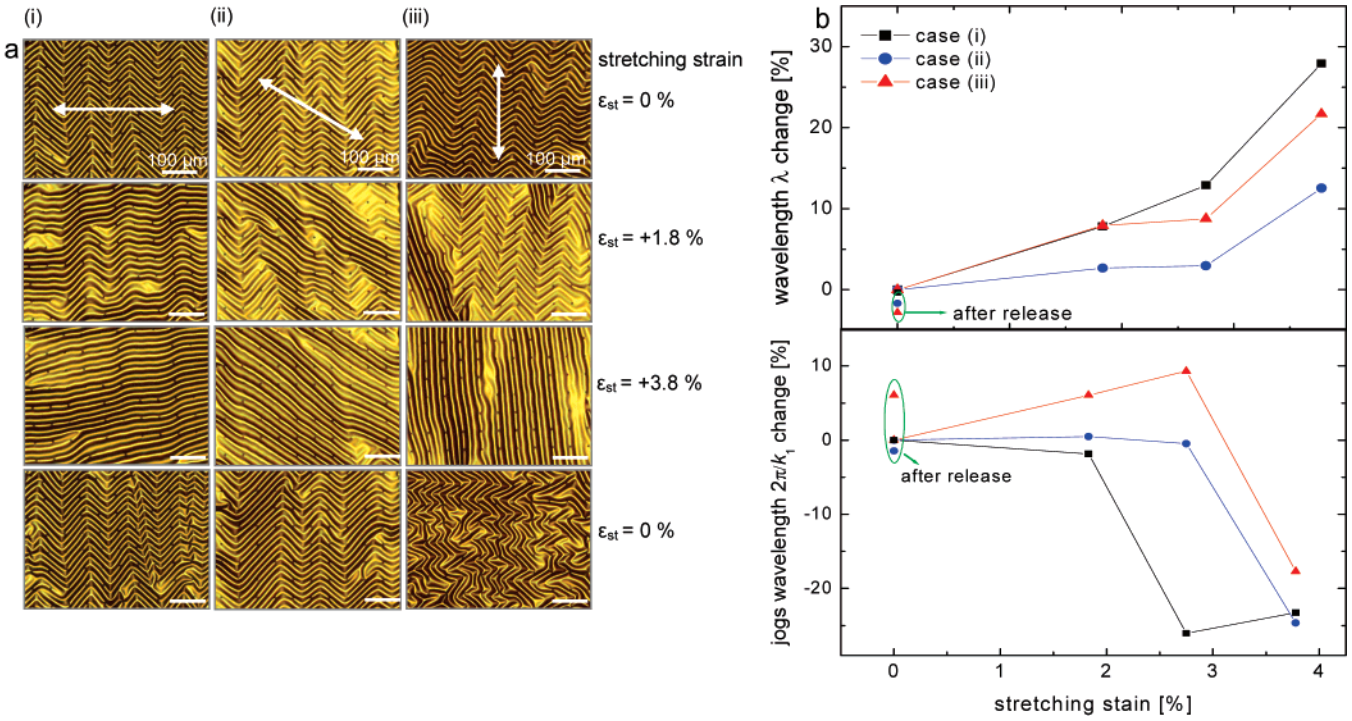

Figure 5. (a) Optical micrographs of 2D wavy Si nanomembranes under different uniaxial strains, applied at three different orientations. These samples consist of Si membranes with thicknesses of 100 nm on PDMS, formed with a thermal prestrain of 3.8%. The images were collected in the relaxed state before stretching (top frames), the relaxed state after stretching (bottom frames), and at uniaxial applied tensile strains of 1.8% (top middle frames) and 3.8% (bottom middle frames). (b) Dependence of the short wavelength on applied strain in the three different directions.

and 17.2 μm for $\epsilon_{st} = 0$, 1.8, and 3.8%, which confirms that the short wavelength increases with the applied strain, as observed in experiments. For case iii, both λ and $2\pi/k_1$ increased with applied stretching strain, since waves were relaxed along the direction of stretching strain, and the jogs angle (θ) was not changed significantly by the Poisson effect. The biaxial stretchability of the buckled membranes was also investigated by thermally induced tensile strains (Figure S6). The herringbone waves generated by thermal strain slowly disappeared as the sample was heated; they recovered completely upon cooling.

These observations apply only to the central regions of the membranes. As indicated in the bottom frames of Figure 1, the edges of the membranes show 1D wave structures with wavevectors oriented along the edges. AFM images and linecut profiles of the edge region, the central region, and the transition area between them are shown in Figure 6. The 1D waves that originate near the edge of the Si (top frame) gradually become bent (middle frame) until they transform into the herringbone geometries in the central regions (bottom frame). The λ values in these regions are 16.6, 13.7, and 12.7 μm, respectively (from top frame), with A_1 of 0.52, 0.55, and 0.67 μm. Compared to the 1D waves at the edges, the 2D herringbone waves have smaller λ and A_1, suggesting that the inner area of Si is affected more strongly by the compressive strain than the edges. The stress state near the edge is approximately uniaxial compression within some distance range because of the traction-free edge of the membrane. This uniaxial compression is parallel to this free

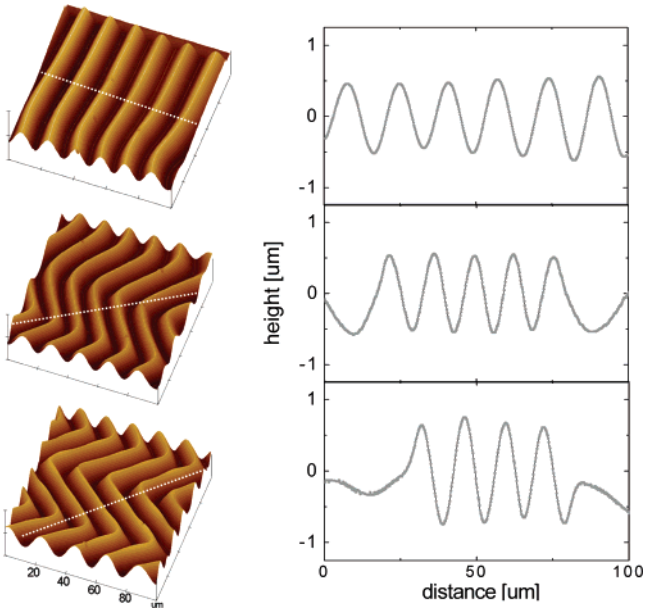

Figure 6. AFM images of different regions of a 2D wavy Si nanomembrane, showing the 1D wavy geometry characteristics of a region near the edge of the membrane (top frame), a region slightly removed from this edge area (middle frame), and a region near the center of the membrane (bottom frame). The sample consisted of a Si membrane with thickness of 100 nm on PDMS, formed with a thermal prestrain of 3.8%.

edge and therefore leads to 1D waves along the edge. The stress state, however, becomes equi-biaxial compressive in the central region where herringbone structures result. For

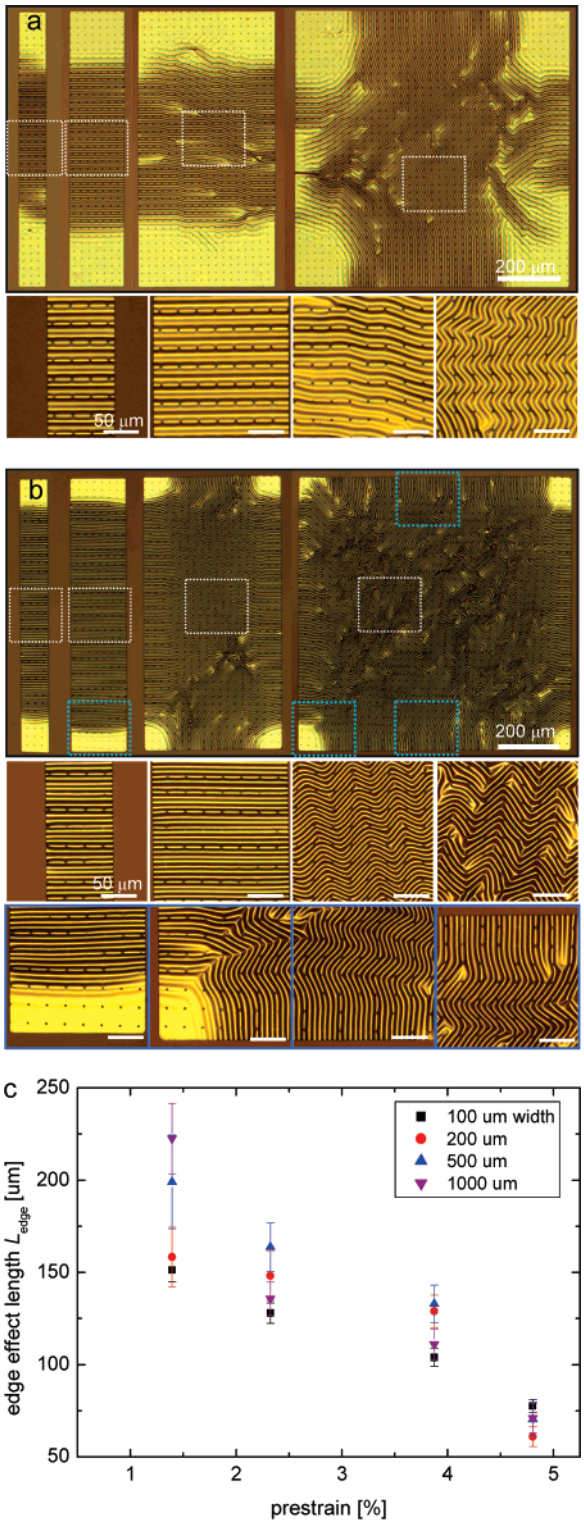

Figure 7. Optical micrographs of 2D wavy Si nanomembranes with lengths of 1000 μm and with widths of 100, 200, 500, and 1000 μm. These membranes all have thicknesses of 100 nm and were formed on the same PDMS substrate with thermal prestrains of (a) 2.3% and (b) 4.8%. (c) Dependence of the edge effect length on prestrain for similar membranes.

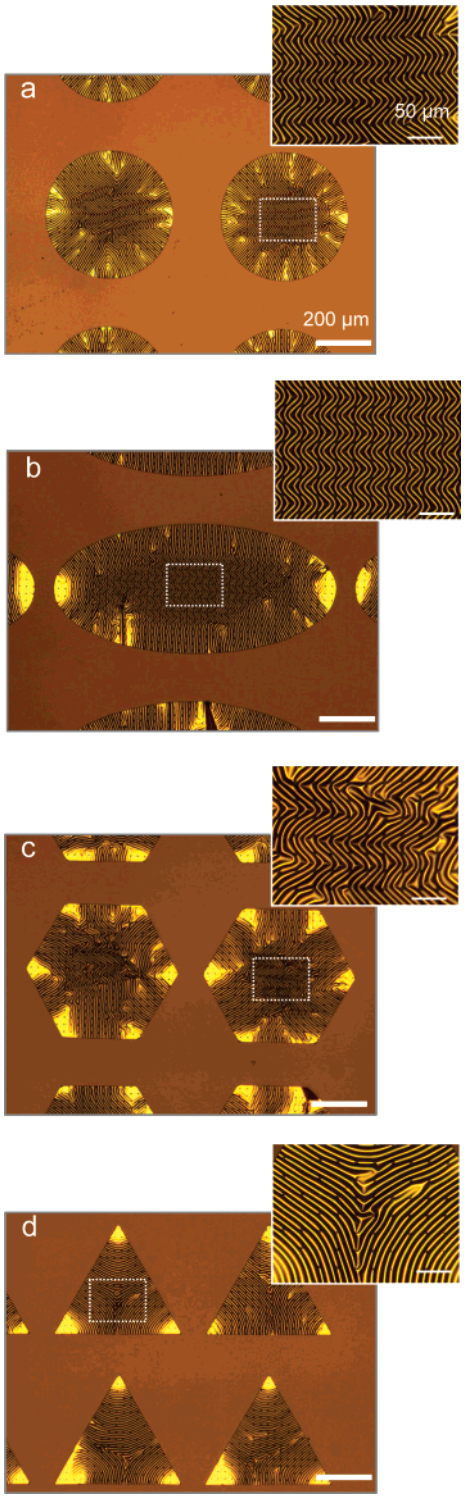

Figure 8. Optical micrographs of 2D wavy Si nanomembranes with different shapes: (a) circle, (b) oval, (c) hexagon, and (d) triangle. These membranes all have thicknesses of 100 nm and were formed on PDMS with a thermal prestrain of 4.8%.

the transition area between the 1D wavy edge and the herringbone waves, the unbalanced biaxial compression causes a "semi"-herringbone wave with the large jog angle. Our model yields λ and A_1 of 16.9 and 0.83 μm, respectively, for the 1D waves and 12.4 and 0.90 μm for the herringbone structure. These results agree reasonably well with the experimentally observed values.

To investigate further these edge effects, we fabricated rectangular membranes with lengths of 1000 μm and with widths of 100, 200, 500, and 1000 μm, all on the same PDMS substrate. Figure 7 shows optical micrographs of these

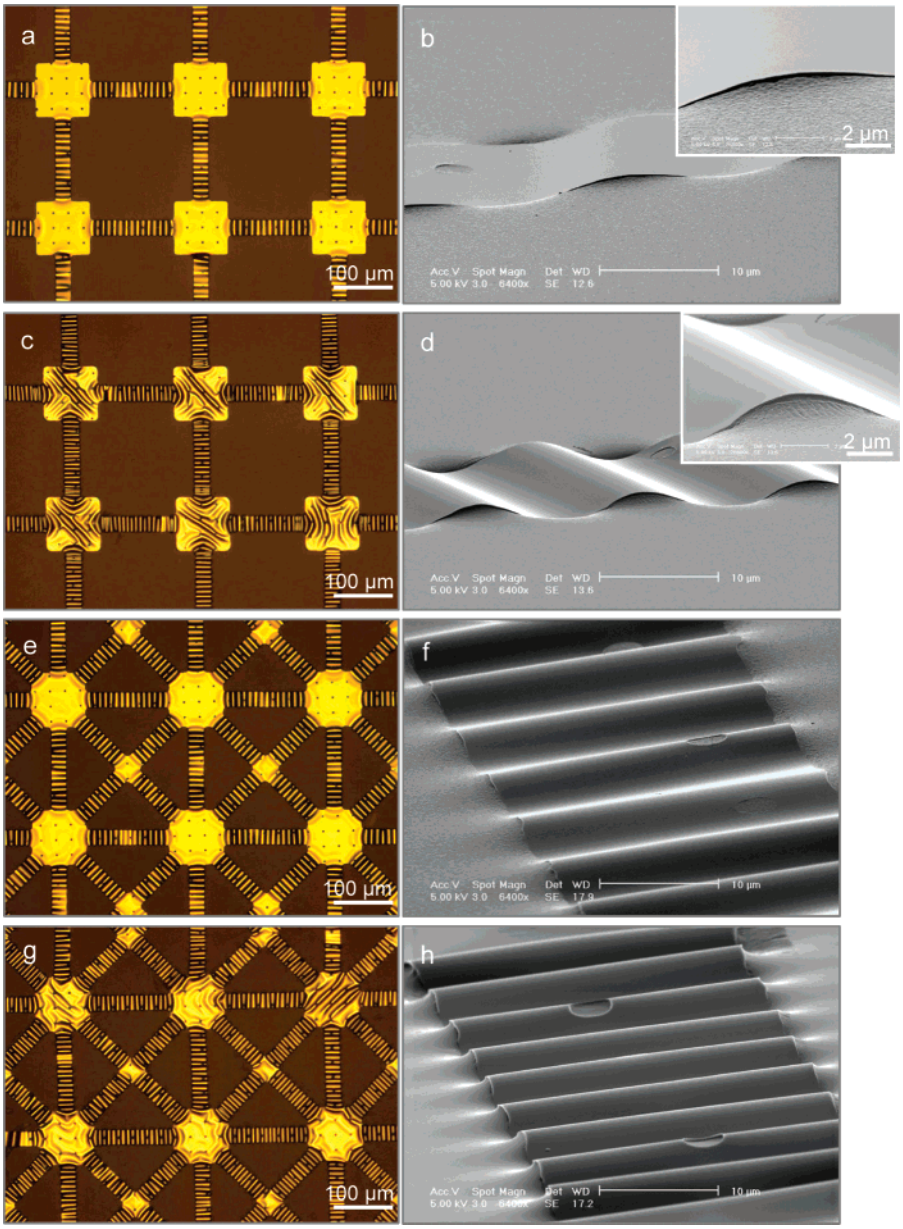

Figure 9. Optical micrographs of wavy structures of Si nanomembranes with shapes designed to exploit edge effects to provide 2D stretchability in interconnected arrays of flat islands. In both cases illustrated here, the Si is 100 nm thick, the squares are 100 × 100 μm, and the ribbon connections are 30 × 150 μm lines. The prestrain is (a, e) 2.3% and (c, g) 15%. SEM images (tilt angle of 75°) of selected regions that show ribbons and squares of (a, c, e, g) are shown in (b, d, f, h), respectively. The insets of high-magnification SEM images show the raised region of waves in b and d.

structures, for two different levels of thermal prestrain. At low thermal prestrain (ca. 2.3%, Figure 7a), the 100 and 200 μm wide membranes exhibit perfect 1D waves from one side to the other, with flat, undeformed regions at the ends. The 500 μm wide membrane shows similar 1D waves and flat regions, but the waves have slightly bent geometries in the middle of the structures, with overall ordering and uniformity in orientation that are substantially less than the 100 and 200 μm cases. For the 1000 μm square, 1D waves are present in the central regions of the edges, with flat areas in the corners. The center part of the membrane shows fully developed herringbone geometries. For the corner flat region, there is an approximately stress-free state due to the two free edges. No waves form near such corners. With increasing prestrain (4.8%, Figure 7b), the flat regions in all cases decrease in size. 1D wavy behavior persists in the 100 and 200 μm ribbons, but pronounced herringbone morphologies appear in the central region of the 500 μm case. At the higher prestrain, equi-biaxial compressive strains are present in the inner region of 500 μm wide membrane. For the 1000 μm square membrane, the herringbone behavior extends to regions close to the edges. The characteristic length scales that define the spatial extent of the flat regions, which we refer to as the edge effect length, L_{edge}, can be evaluated as a function of membrane size and prestrain. Figure 7c shows results that indicate a linear scaling of this length with

prestrain, in a manner that is independent of the size of the membrane, for the cases investigated here. As the prestrain becomes higher, the length of uniaxial strain region becomes smaller. Therefore, shorter range 1D waves form and similar behavior can be observed in the stress-free regions near the two free edges.

Figure 8 shows optical micrographs of wavy structures that form in other membrane geometries, including circles, ovals, hexagons, and triangles. The results are qualitatively consistent with observations in the ribbons and squares of Figure 7. In particular, the edge regions show 1D waves oriented parallel to the edges. Waves with the orthogonal orientation only appear at distances larger than the L_{edge} from the edge. For the circle, 1D waves appear near the edges, with an overall radial orientation due to the shape of the membrane. Herringbone waves appear in the center. The ovals exhibit similar behavior, although with flat regions at the edges of the major axis, due to the small radius of curvature in these regions. For the hexagon and triangle shapes, the sharp corners (angles of 120° and 60°, respectively), lead to flat regions. Herringbone geometries appear in the center of the hexagons. The centers of the triangles show the merging of 1D waves, for the level of prestrain shown here. For shapes with clear corners (e.g., hexagon, triangle, and tip of ellipse), there is no wave near the corner because the two intersecting free edges (not necessarily perpendicular) give a stress-free state. For the triangle shape, there is not enough space to generate the herringbone structure even in the central region.

The membranes themselves provide a path to biaxially stretchable electronic devices. The edge effects outlined above can be exploited to realize a particular outcome that might be useful for certain classes of such devices. In particular, in an imaging system, there might be value in maintaining flat, undeformed regions at the locations of the photodetectors to avoid nonideal behavior that occurs when these devices have wavy shapes.[7b] Figure 9 presents some representative examples of stretchable membranes that achieve this outcome. These structures consist of 100 × 100 μm square islands connected by 30 μm × 150 μm ribbons (30 μm × 210 μm for orthogonal ribbons) in the vertical and horizontal directions (Figure 9a,c), and in the vertical, horizontal and diagonal directions (Figure 9e,g). Changes in the amplitudes and wavelengths of the waves in the ribbons provide a means to accommodate applied strains, in a manner that largely avoids deformations in the regions of the square islands. We examined the behavior of these structures at several different applied strains. Parts a and e of Figure 9 show representative cases in the low strain (ca. 2.3%) regime, applied by heating the samples in an oven. Parts c and g of Figure 9 show the same structures at relatively high biaxial strains (ca. 15%), applied using a mechanical stage. As is evident, in the low-strain regime the islands remain flat; at sufficiently high strains, wave structures begin to form in these regions. Good adhesion between PDMS and Si was maintained at all strains, as shown in the tilted angle SEM images (Figure 9b,d,f,h). The insets of high-magnification SEM image in parts b and d of Figure 9 also confirm the strong bond of Si with PDMS.

In summary, nanomembranes of silicon can be integrated with prestrained elastomeric substrates to create 2D "wavy" structures with a range of geometries. Many aspects of the mechanical behavior of these systems are in good agreement to theoretically predicted behaviors. These results might be useful for envisioned applications of electronics in systems where full stretchability is required during use or during installation.

Acknowledgment. We thank T. Banks and K. Colravy for help with processing using facilities at the Frederick Seitz Materials Research Laboratory. This material is based upon work supported by the National Science Foundation under Grant DMI-0328162 and the U.S. Department of Energy, Division of Materials Sciences under Award No. DEFG02-91ER45439, through the Frederick Seitz MRL and Center for Microanalysis of Materials at the University of Illinois at Urbana-Champaign. Dr. W. M. Choi would like to thank to Korea Research Foundation for the postdoctoral fellowship support (KRF-2005-214-D00261), funded by the Korean Government (MOEHRD).

Supporting Information Available: Additional experimental data about the various images on different spots of sample, the relation of Si strain and thermal prestrain, the repeated stretching cycle test, and the biaxial stretching test by the heating sample. This material is available free of charge via the Internet at http://pubs.acs.org.

References

(1) (a) Reuss, R. H.; Chalamala, B. R.; Moussessian, A.; Kane, M. G.; Kumar, A.; Zhang, D. C.; Rogers, J. A.; Hatalis, M.; Temple, D.; Moddel, G.; Eliasson, B. J.; Estes, M. J.; Kunze, J.; Handy, E. S.; Harmon, E. S.; Salzman, D. B.; Woodall, J. M.; Alam. M. A.; Murthy, J. Y.; Jacobsen, S. C.; Olivier, M.; Markus, D.; Campbell, P. M.; Snow, E. *Proc. IEEE* **2005**, *93*, 1239. (b) Jain, K.; Klosner, M.; Zemel, M.; Raghunandan, S. *Proc. IEEE* **2005**, *93*, 1500. (c) Nathan, A.; Park, B. K.; Ma, Q. H.; Sazonov, A.; Rowlands, J. A. *Microelectron. Reliab.* **2002**, *42*, 735.

(2) Someya, T.; Sekitani, T.; Iba, S.; Kato, Y.; Kawaguchi, H.; Sakurai, T. *Proc. Natl. Acad. Sci. U.S.A.* **2004**, *101*, 9966.

(3) (a) Hsu, P. H. I.; Huang, M.; Gleskova, H.; Xi, Z.; Suo, Z.; Wagner, S.; Sturm, J. C. *IEEE Trans. Electron. Dev.* **2004**, *51*, 371. (b) Jin, H. C.; Abelson, J. R.; Erhardt, M. K.; Nuzzo, R. G. *J. Vac. Sci. Technol., B: Microelectron. Nanometer Struct.-Process., Meas., Phenom.* **2004**, *22*, 2548.

(4) Nathan, A.; Park, B.; Sazonov, A.; Tao, S.; Chan, I.; Servati, P.; Karim, K.; Charania, T.; Striakhilev, D.; Ma, Q.; Murthy, R. V. R. *Microelectron. J.* **2000**, *31*, 883.

(5) (a) Someya, T.; Kato, Y.; Sekitani, T.; Iba, S.; Noguchi, Y.; Murase, Y.; Kawaguchi, H.; Sakurai, T. *Proc. Natl. Acad. Sci. U.S.A.* **2005**, *103*, 12321. (b) Lacour, S. P.; Jones, J.; Wagner, S.; Li, T.; Suo, Z. G. *Proc. IEEE* **2005**, *93*, 1459. (c) Lacour, S. P.; Wagner, S.; Huang, Z. Y.; Suo, Z. *Appl. Phys. Lett.* **2003**, *82*, 2404.

(6) Khang, D.-Y.; Jiang, H.; Huang, Y.; Rogers, J. A. *Science* **2006**, *311*, 208.

(7) (a) Sun, Y.; Kumar, V.; Adesida, I.; Rogers, J. A. *Adv. Mater.* **2006**, *18*, 2857. (b) Sun, Y.; Choi, W. M.; Jiang, H.; Huang, Y.; Rogers, J. A. *Nat. Nanotechnol.* **2007**, *1*, 201.

(8) (a) Ouyang, M.; Yuan, C.; Muisener, R. J.; Boulares, A.; Koberstein, J. T. *Chem. Mater.* **2000**, *12*, 1591. (b) Childs, W. R.; Nuzzo, R. G. *J. Am. Chem. Soc.* **2002**, *124*, 13583. (c) Efimenko, K.; Wallace, W. E.; Genzer, J. *J. Colloid Interface Sci.* **2002**, *254*, 306. (d) Hillborg,

H.; Tomczak, N.; Olah, A.; Schonherr, H.; Vancso, G. J. *Langmuir* **2004**, *20*, 785.
(9) (a) Buma, T.; Spisar, M.; O'Donnell, M. *Appl. Phys. Lett*. **2001**, *79*, 548. (b) *Properties of Silicon*; INSPEC: New York, 1998. The coefficients of thermal expansion are $\alpha_{PDMS} = 3.1 \times 10^{-4}$ K^{-1} and $\alpha_{Si} = 2.6 \times 10^{-6}$ K^{-1} for PDMS substrate and Si nanomembrane, respectively. The thermal prestrain for the samples prepared at 150 °C was calculated by $\Delta\alpha\ \Delta T = (3.1 \times 10^{-4} - 2.6 \times 10^{-6})(150 - 25) = 3.8\%$.
(10) Timoshenko, S. *Theory of Plates and Shells;* McGraw-Hill: New York, 1940.
(11) Timoshenko, S.; Goodier, J. N. *Theory of Elasticity*, 3rd ed.; McGraw-Hill: New York, 1969.
(12) (a) Chen, X.; Hutchinson, J. W. *J. Appl. Mech. Trans. ASME* **2004**, *71*, 597. (b) Chen, X.; Hutchinson, J. W. *Scr. Mater*. **2004**, *50*, 797.
(13) Huang, Z. Y.; Hong, W.; Suo, Z. *J. Mech. Phys. Solids* **2005**, *53*, 2101.
(14) Bietsch, A.; Michel, B. *J. Appl. Phys.* **2000**, *88*, 4310.
(15) (a) Ohzono, T.; Shimomura, M. *Phys. Rev. B* **2004**, *69*, 132202. (b) Ohzono, T.; Shimomura, M. *Langmuir* **2005**, *21*, 7230.

NL0706244